

## Article

# Impact of Material on Response and Calibration of Particle Number Systems

Barouch Giechaskiel \* and Anastasios Melas 

Joint Research Centre (JRC), European Commission, 21027 Ispra, Italy

\* Correspondence: barouch.giechaskiel@ec.europa.eu; Tel.: +39-0332-78-5312

**Abstract:** In Europe and Asia, vehicle emissions regulations include a number limit for particles larger than 23 nm, which might be reduced to 10 nm in the future. A particle number system (LABS) consists of a volatile particle remover (VPR) and a particle number counter (PNC). However, it is not simple to derive the combined penetration (efficiency), because the parts are calibrated separately at different sizes and with different materials. On the other hand, portable emissions measurement systems (PEMS) for real-driving emissions (RDE) testing or counters for periodical technical inspection (PTI) of vehicle exhaust are calibrated as complete units with soot-like aerosol. The aim of this study is to estimate the efficiency of a LABS using different materials (soot, graphite, salt, silver, emery oil), typically used for the calibration of LABS, PEMS or PTI counters. The results show that appropriate selection of the calibration material is important in order to have representative of the reality efficiencies. The impact is very high for 23 nm systems, but less critical for 10 nm systems. The estimation of a mean size based on the ratio of 23 nm and 10 nm measurements and the correction of the losses in the sub-23 nm region are also discussed.

**Keywords:** particle number; calibration; PNC; VPR; catalytic stripper; penetration; efficiency; soot; salt; silver



**Citation:** Giechaskiel, B.; Melas, A. Impact of Material on Response and Calibration of Particle Number Systems. *Atmosphere* **2022**, *13*, 1770. <https://doi.org/10.3390/atmos13111770>

Academic Editor: Kenichi Tonokura

Received: 7 October 2022

Accepted: 25 October 2022

Published: 27 October 2022

**Publisher's Note:** MDPI stays neutral with regard to jurisdictional claims in published maps and institutional affiliations.



**Copyright:** © 2022 by the authors. Licensee MDPI, Basel, Switzerland. This article is an open access article distributed under the terms and conditions of the Creative Commons Attribution (CC BY) license (<https://creativecommons.org/licenses/by/4.0/>).

## 1. Introduction

Particle number measurements are part of the European Union (EU)-type approval regulations since 2011 for light-duty diesel vehicles [1]. Over the years, limits were added to light-duty direct injection gasoline vehicles, heavy-duty engines and non-road mobile machinery (i.e., off-road engines). Many countries in Asia have also included the particle number limits in their regulations [2]. All regulations prescribe non-volatile particles (i.e., that do not evaporate at 350 °C) above 23 nm. A similar methodology was also included in the aviation sector, with the main difference the lower size (10 nm instead of 23 nm) [3]. Concerns for existence of non-volatile particles below 23 nm for vehicles led to investigations and expansion of the vehicle emissions regulation protocol down to 10 nm [4]. The new methodology, included in the global technical regulation (GTR 15), is not part of any vehicle regulation yet, but there are discussions on-going to include them in the next EU regulatory step (Euro 7) for both light-duty and heavy-duty vehicles [5–8].

In addition to the laboratory measurements, since 2017 on-road measurements with portable emissions measurement systems (PEMS) are required [9]. PEMS are smaller and lighter than the laboratory counterparts, but comparable in terms of performance [10]. The current technical requirements prescribe a 23 nm lower cut-off size, but in light of the upcoming regulations, the technical specifications for the 10 nm PEMS are also ready [2].

Recently, a particle number requirement was added during the periodic technical inspection (PTI) of diesel vehicles in some European countries [11–14]. These instruments are typically small handheld counters, robust enough for the environment of garages.

The regulations describe the main technical requirements of the instruments, but there is some degree of freedom for their design. Due to the different complexity levels,

the technical requirements of laboratory, PEMS and PTI instruments are different. The calibration requirements are also included, but not with many details. The latest documents for the laboratory systems were published in 2007 [15,16] and have not been updated since then. PEMS have different calibration procedures, making the direct comparison of laboratory and on-board systems difficult. While soot particles are typically used for laboratory and on-board systems, salt is preferred for PTI instruments.

Studies comparing 23 nm laboratory systems [17–21], and recently a limited number of studies assessing 10 nm systems [22,23], have found, in most cases, good agreement between the systems; but not always [24]. Theoretical studies have presented sources of uncertainty, such as the particle losses inside the system, and the unknown size of the measured exhaust aerosol [10]. Much discussion has also taken place about the calibration material, which is not well defined in the regulations [25]. With a few exceptions, based on theoretical data, most studies investigated parts of the particle number system [26–28]. For this reason, a complete picture is lacking. For laboratory systems, the technical requirements are given for each part, i.e., the pre-conditioning system and the counter. For PEMS and PTI instruments, the requirements are given for the complete unit. There is only a small overlap between the calibration sizes and the direct comparison of the instruments, especially laboratory and PEMS, is difficult. Studies comparing them show acceptable differences [24,29,30], but there is room for improvement. Big differences can be found in the sub-23 nm range, due to the different penetration curves of the systems in that region [24].

The aim of this study is to fully characterize a laboratory particle number system, calibrating its parts separately, but the whole unit as well, with different materials. The experimental results are compared with theoretical calculations. As both 23 nm and 10 nm counters are included, expressions to estimate the mean size and/or to correct for particle losses are also presented.

## 2. Materials and Methods

The calibration setup consisted of a particle generator, a size classifier to select the appropriate size, the reference and the instruments under evaluation. The following sections describe the parts, starting from the instruments under evaluation and concluding with the particle generators.

### 2.1. Description of LABS

The most critical technical specifications of particle number systems are depicted in Figure 1. A laboratory particle number system (LABS) consists of a volatile particle remover (VPR) and a particle number counter (PNC). The VPR dilutes and thermally conditions the sample (removes volatile particles). It has a hot first dilution stage (temperature  $\geq 150$  °C), a catalytic stripper (CS) at 350 °C, and a secondary dilution at ambient temperature to cool down the diluted sample. The PNC, which is based on the condensation particle counting (CPC) technique counts the particles. At the time of writing, all vehicle regulations require counting from approximately 23 nm, except the aviation sector which requires counting from 10 nm. Future vehicle regulations will require a lower detection limit of 10 nm. The CS in the VPR is obligatory for the future 10 nm systems, while 23 nm systems may use a simple evaporation tube instead. Details can be found elsewhere [2].

Figure 1 also presents the main calibration requirements of a LABS. For the VPR, a particle concentration reduction factor (*PCRF*) is determined for 100 nm, 50 nm, 30 nm and 15 nm (only 10 nm systems). This *PCRF* includes the dilution and the particle losses. The ratio of *PCRFs* to the 100 nm *PCRF* have to be lower than threshold values: 2.0 for 15 nm, 1.3 for 30 nm, 1.2 for 50 nm. The counting efficiencies of the 23 nm PNCs ( $PNC_{23}$ ) at 23 nm and 41 nm have to be 50% ( $\pm 12\%$ ) and  $>90\%$ , respectively. The counting efficiencies of the 10 nm PNCs ( $PNC_{10}$ ) at 10 nm and 15 nm have to be 65% ( $\pm 15\%$ ) and  $>90\%$  respectively. The material is not clearly specified. It has to be thermally stable for the VPR calibration, soot-like or emery oil for the  $PNC_{10}$ , but is not prescribed for  $PNC_{23}$ . Finally, it should be

mentioned that the sizes required for calibration of PNCs and VPRs have small overlap. For VPR the sizes are 15 nm, 30 nm, 50 nm and 100 nm; for PNC<sub>23</sub> the sizes are 23 nm and 41 nm; and for PNC<sub>10</sub> they are 10 nm and 15 nm.

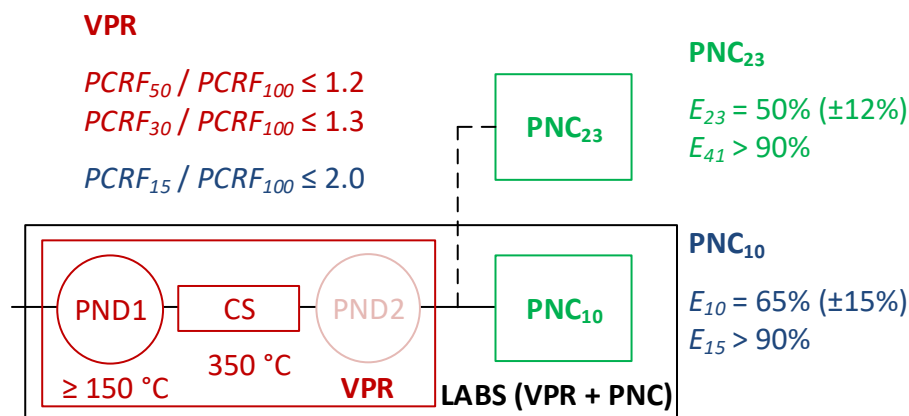


**Figure 1.** Schematic of a typical particle number system (LABS = VPR + PNC in black box) consisting of a VPR (red box) and a PNC (green box). At the top of the figure the main calibration requirements are given for the 23 nm systems; the requirements for the 10 nm systems are shown in blue. *E* = counting efficiency; *PCR<sub>F</sub>* = particle concentration reduction factor; PNC = particle number counter; PND = particle number diluter; CS = catalytic stripper; VPR = volatile particle remover.

The LABS of this study had a VPR with CS and two PNCs counting from 23 nm and 10 nm, respectively. In some cases, the combined LABS will be called VPR + PNC. Appropriate “size” indexes (23 or 10) will be used whenever reference to a specific combination is made.

### 2.2. Calibration Setups

The calibration tests included monodisperse, i.e., with specific sizes, calibration of the PNCs or the complete system LABS (VPR + PNC) (Figure 2), monodisperse calibration of the VPR (Figure 3), and polydisperse, i.e., with the whole particle size distribution, checks of the complete system LABS (Figure 4). The particle generators will be described in a subsequent section. The reference instrument (PNC<sub>Ref</sub>) was the butanol based CPC (model 3752) from TSI (Shoreview, MN, USA), with lower detection limit 4 nm [31,32]. The maximum concentration in single counting mode was  $10^5 \text{ \#/cm}^3$ . The lengths of the tubes were selected such as to have similar diffusion losses between the reference and test instruments.

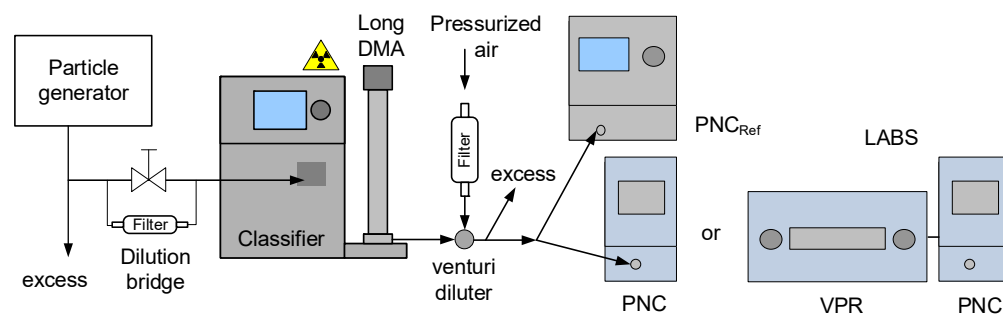


**Figure 2.** Experimental setup for monodisperse calibration of the PNC and complete LABS (VPR + PNC) system. DMA = differential mobility sizer; PNC = particle number counter; VPR = volatile particle remover.

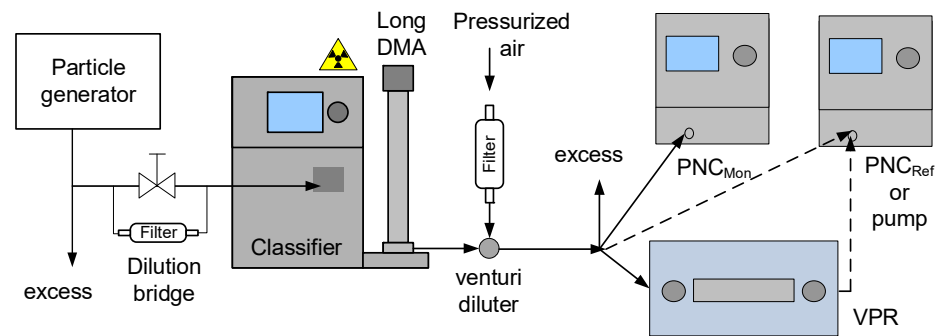


**Figure 3.** Experimental setup for the monodisperse calibration of the VPR. DMA = differential mobility sizer; PNC = particle number counter; VPR = volatile particle remover.

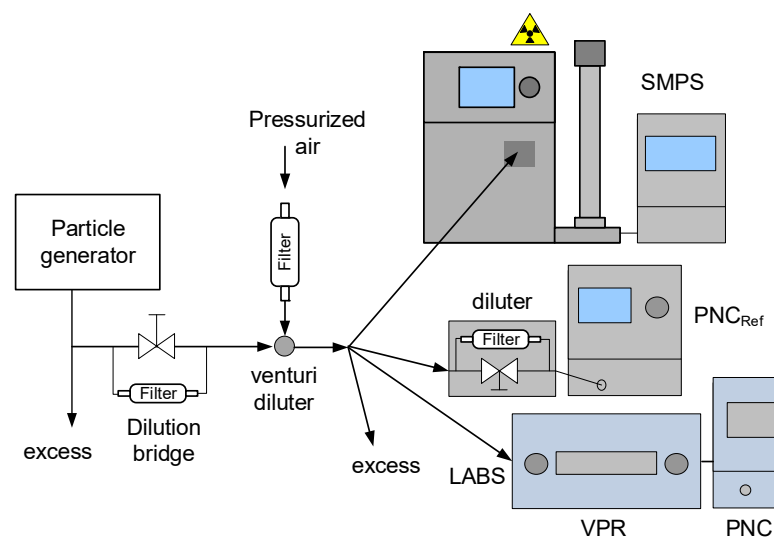


**Figure 4.** Experimental setup for the polydisperse check (validation) of the VPR + PNC system. PNC = particle number counter; VPR = volatile particle remover.

### 2.2.1. Monodisperse Calibration of PNC or LABS

The setup of Figure 2 was used. The polydisperse generated particles were size selected in a classifier (model 3081 from TSI). The classifier included a neutralizer (model 3077A from TSI) and a long differential mobility analyzer (DMA). The dilution upstream of the classifier was a simple dilution bridge (i.e., bifurcated diluter), and was adjusted in order to have monodisperse concentrations at the outlet of the classifier for each size tested  $<10^5 \text{ \#/cm}^3$ . The sizes set were 7.5 nm, 10 nm, 15 nm, 23 nm, 30 nm, 41 nm, 50 nm and 100 nm. The flowrate in the classifier, around 1 L/min, was controlled by an in-house made venturi (ejector) diluter at the outlet of the classifier, that also provided adequate flow for all instruments: the reference PNC ( $\text{PNC}_{\text{Ref}}$ ) and the test PNC (23 nm or 10 nm) or the complete system (LABS). The monodisperse efficiency  $E$  at each size  $i$  was calculated as:

$$E_{\text{mono},i,\text{PNC}} = C_{\text{PNC},i} / C_{\text{PNC,Ref},i} \quad (1)$$

$$E_{\text{mono},i,\text{LABS}} = C_{\text{LABS},i} / C_{\text{PNC,Ref},i} \quad (2)$$

where  $C$  is the concentration ( $\text{\#/cm}^3$ ) measured by the respective instrument at size (diameter)  $i$  (nm) set at the classifier.

### 2.2.2. Monodisperse Calibration of VPR

The setup for the monodisperse calibration of the VPR (Figure 3) was the same as for the monodisperse calibration of the PNC, with the addition of a PNC ( $\text{PNC}_{\text{Mon}}$ ) monitoring

the concentrations at the outlet of the venturi diluter, when the  $PNC_{Ref}$  was exchanging positions (upstream and downstream of the VPR) with a pump of equal flow.

The  $PCRF$  at each size was calculated as:

$$PCRF_i = C_{PNC,Ref,i,upstream} / C_{PNC,Ref,i,downstream} \quad (3)$$

The  $PCRF$  ratios of different sizes to 100 nm were calculated as:

$$PCRF_{ratio,i} = PCRF_i / PCRF_{100} \quad (4)$$

The LABS is correcting the measured concentrations with the average  $PCRF$  of 30, 50 and 100 nm, which is calculated as follows:

$$PCRF_{ave} = (PCRF_{30} + PCRF_{50} + PCRF_{100}) / 3 \quad (5)$$

The monodisperse efficiency of the VPR at a size  $i$  was calculated as:

$$E_{mono,i,VPR} = PCRF_{ave} / PCRF_i \quad (6)$$

Note that the VPR efficiency can take values slightly higher than unity, because the  $PCRF$  at 100 nm is lower than the average one.

### 2.2.3. Polydisperse Checks of LABS

The polydisperse checks (Figure 4) were performed by simultaneously measuring the polydisperse size distributions generated and appropriately diluted using LABS and the reference instrument [33]. The  $PNC_{Ref}$  was additionally connected to a bifurcated diluter model DDS 560 from TOPAS (Dresden, Germany) in order to keep the concentration in the single particle counting mode. For these tests the soot, graphite, silver and salt generators were used, plus an idling Diesel vehicle. The produced geometric mean diameters (GMDs) ranged from 30 nm up to 110 nm and the geometric standard deviations (GSDs) from 1.6 to 2.1, as checked with a scanning mobility particle sizer (SMPS) measuring in parallel with the rest instruments.

The efficiency was determined as:

$$E_{poly,GMD,LABS} = C_{LABS} / C_{Ref,corr} \quad (7)$$

where  $C_{Ref,corr}$  is the concentration of the reference instrument corrected for the dilution ratio and any particle losses in the diluter (around 25% at the 10–15 nm range).

### 2.2.4. Estimation of Efficiencies (Fittings)

When enough data were available, curves were fitted to the experimental (monodisperse) data. The fitted curves were then used to estimate the response of the complete LABS either with monodisperse or polydisperse aerosol. For PNC and VPR, the following equations were applied:

$$E_{mono,i} = s - s \times \exp [ \ln 2 \times (d_0 - d_i) / (d_{50\%} - d_0) ] \quad (8)$$

$$E_{mono,i,norm} = E_{mono,i} \times k \quad (9)$$

where  $d_0$  (nm) and  $d_{50\%}$  (nm) are the diameters with efficiency 0% and 50%, respectively,  $s$  (–) the efficiency at the plateau region,  $k$  (–) the calibration factor: for PNCs it is the inverse of the slope; for VPRs it is  $PCRF_{100} / PCRF_{ave}$ . The  $k$  factors were not applied, in order to take into account the impact of the material on the results.

The efficiency of the complete system (LABS) is given by:

$$E_{mono,i,LABS} = E_{mono,i,norm,PNC} \times E_{mono,i,norm,VPR} \quad (10)$$

The estimated efficiency of LABS is also abbreviated as “VPR × PNC”, while the measured efficiency of the LABS is abbreviated as “VPR + PNC”.

The estimated polydisperse efficiency ( $E_{poly}$ ) of the LABS for a size distribution with a specific GMD and GSD was calculated by integrating the monodisperse efficiencies at each size for the specific size distribution.

### 2.2.5. Sub-23 nm Particles and GMD

In order to assess whether the ratio of the 10 nm and 23 nm systems ( $LABS_{10}/LABS_{23}$ ) can give an estimation of the GMD of the measured size distributions, the experimental data were also compared with theoretically estimated ratios ( $E_{poly,10}/E_{poly,23}$ ) for the specific GMD (and GSD).

### 2.2.6. Corrected 10 nm Concentration

The losses in the VPR are taken into account with the average  $PCRF$  (Equation (5)), which considers only 30 nm, 50 nm and 100 nm losses. The 10 nm systems can have big differences below 30 nm: there is a maximum  $PCRF$  ratio of 15 nm to 100 nm of two, but no lower limit. Thus, the losses in the sub-30 nm range can be up to 50% compared to the >30 nm range. The following equation has been proposed to calculate the corrected 10 nm concentration [34]:

$$C_{LABS,10,corr} = C_{LABS,23} + C_{LABS,10-23,corr} \quad (11)$$

$$C_{LABS,10-23,corr} = (C_{LABS,10} - C_{LABS,23}) \times PCRF_{15}/PCRF_{ave} \quad (12)$$

where:

$$C_{LABS,23} = C_{PNC,23} \times k_{PNC,23} \times PCRF_{ave} \quad (13)$$

$$C_{LABS,10} = C_{PNC,10} \times k_{PNC,10} \times PCRF_{ave} \quad (14)$$

where  $k$  (–) the calibration factor of the PNCs (inverse of the slope).

### 2.2.7. Uncertainty of Measurement

The uncertainty of measurements depends mainly on the uncertainty of the reference instrumentation. Other sources, such as flow splitting, diffusion losses in the tubes can also contribute. For the monodisperse PNC tests, we estimated an uncertainty of 5–10% due to the uncertainty of the reference instrument, the flowmeters and the splitter bias. For the monodisperse VPR and LABS tests the uncertainty was 10–15% due to the additional uncertainty of the linearity of the reference system (when measuring upstream and downstream) and the pressure differences at the two locations (upstream and downstream). For the polydisperse LABS tests the uncertainty of the diluter was also considered for the PNC. Even though it was calibrated, it had a 5–15% uncertainty, in particular, at low sizes where the particle losses were high. Thus, the uncertainty of the polydisperse tests was around 10–20%. These values should be kept in mind when discussing the results.

## 2.3. Particle Generators

The following generators were assessed in this study:

Silver particles were generated with a silver particle generator (SPG) from Catalytic Instruments (Rosenheim, Germany) [31]. Silver was heated and evaporated in a tube at 1100 °C, and a 2 L/min particle free air transported the silver vapors to the main flow tube, where they were diluted with additional 15 L/min (adjustable by the user) particle free air. For some tests, the particles passed through a catalytic stripper (CS; model CS015 from Catalytic Instruments) heated at 375 °C. The particles will be called “oxidized silver” particles.

Silver particles were also generated with a tungsten glowing wire generator (GWG) with a silver filament around it. The heat from the tungsten wire heated the silver filament, evaporating silver particles. The carrier gas was  $N_2$ , which was also mixed with  $N_2$  to bring down the temperature and the concentration. The particles will be called “silver”

particles. For some tests these particles were thermally pre-treated with the CS before the measurements with the various instruments.

Salt particles were generated in the field calibration system (FCS 249) from TOPAS (Dresden, Germany). The atomized particles were subsequently dried in a tube with silica gel. The particles will be called as “dry salt” particles.

Graphite particles were generated in a spark discharge graphite generator, model DNP 3000 from PALAS (Karlsruhe, Germany) or model VSP-G1 from Vsparticle (Delft, The Netherlands) [35]. High-voltage spark discharges between two graphite electrodes evaporated the electrode material. Nitrogen transferred the vapors to the main flow tube, where further dilution with filtered air reduced the particle number concentration. The particles will be called “graphite” particles.

Soot particles were generated with the AVL particle generator (APG) [36]: a combination of a mini combustion aerosol standard (CAST) model 6.203 C (modified) from Jing Ltd. (Zollikofen, Switzerland) and a thermal conditioning (350 °C) and dilution unit. The conditioning unit followed the same concept as the VPR of the particle number measurement systems. By adjusting the settings of the generator (fuel flow, oxidation air and mixing air), different size distributions could be produced. The particles will be called “soot” particles, and when necessary, it will be clarified if they were sampled directly from the burner, or the VPR, and/or mixing gas was added.

Soot particles were also produced with a Euro 3 Diesel vehicle without Diesel particulate filter (DPF) at idling. The sample was taken before the aftertreatment device (engine out).

Emery oil, i.e., polyalphaolefin (PAO), particles were generated with an electrospray aerosol generator, model EAG 3482 from TSI. The generator produced particles by moving the conductive liquid solution (PAO, ethanol, isopropanol and ammonium acetate) through a capillary and applying an electrical field to the liquid at the capillary tip. The electrical field drew the liquid from the tip into a conical jet from which ultrafine charged droplets were emitted. Air and CO<sub>2</sub> were merged with the droplets, and the liquid evaporated while the charge was neutralized by an ionizer.

### 3. Results and Discussion

#### 3.1. Monodisperse Calibration of PNC

Figure 5a,b presents the monodisperse calibration results for the 10 nm and 23 nm PNCs, respectively. The tests were conducted according to the setup of Figure 2 and the efficiencies were calculated according to Equation (1). Beginning with the PNC<sub>10</sub> and the oxidized silver particles (Figure 5a, open circles), which had the most repetitions, the counting efficiency at 6 nm was slightly above 0, at 7.5 nm around 40–50%, at 10 nm 80% or higher, and at 30 nm or larger sizes 100%. There was practically no difference between thermally treated (with catalytic stripper) oxidized silver particles and non-treated. The difference at 7.5 nm is probably due to experimental uncertainties. The silver particles (asterisks) gave similar results for the limited number of sizes available. The results were very close to the manufacturer’s calibration data with emery oil (PAO) (small lines). Graphite (triangles) and diffusion flame soot (squares) particles had similar results. Salt (diamonds) was the only material that had lower counting efficiencies, around 5–10%. The results are similar to results in the literature: salt particles have lower efficiencies than PAO with differences of 10% at 20 nm [27] and even larger at smaller sizes [27,37]. Our results showed that silver, soot, graphite and PAO were close to each other.

The material had, in general, small impact on the counting efficiencies of the PNC<sub>10</sub>. On the other hand, the impact of the material on the PNC<sub>23</sub> efficiencies was evident (Figure 5b). At 23 nm, for example, the counting efficiency with PAO by the manufacturer was 55%, with salt 0% and with graphite and soot somewhere in between: 27% for graphite, but 20–35% for soot. Regarding soot particles, dry soot after thermal pretreatment had lower counting efficiencies. Adding mixing N<sub>2</sub> in the fuel resulted in higher efficiencies but this could be due to the different oxidation air flow rate: the mixture was lean in the setting

with mixing air, but rich without. In general, the higher the  $\lambda$ , the larger the mean size of the produced size distribution and the elemental carbon fraction [38–41]. Thermal pre-treatment also reduces the organic carbon fraction [42,43]. A study that examined the generator's settings on the counting efficiencies found lower efficiencies with rich mixture [42], in agreement with our results. Another reason for the differences in the counting efficiencies is that the lean setting with the mixing air was bimodal [44], and thus the higher fraction of multiply charged particles might have increased the counting efficiency.

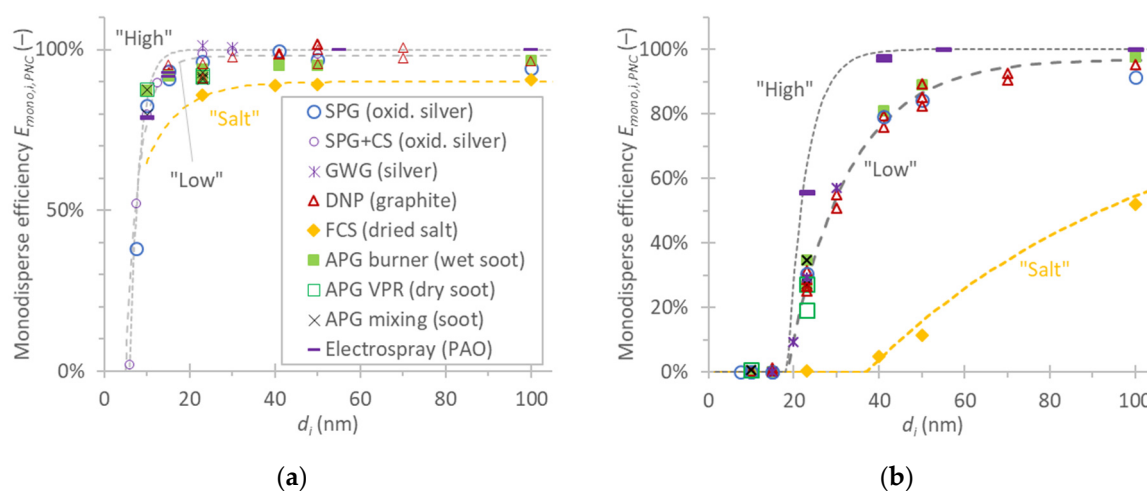


**Figure 5.** Monodisperse calibration of PNCs with various materials: (a) PNC<sub>10</sub>; (b) PNC<sub>23</sub>. Lines give fittings to the experimental data of “high”, “low”, and “salt” efficiencies.

Lower efficiencies of soot compared to PAO have also been reported in the literature [25,27,28,42,45]. The effect of calibration material becomes more pronounced as the temperature difference between the saturator and the condenser decreases [46,47]. Similar soot and graphite efficiencies have been also shown previously [26]. The lower efficiency with salt has been presented as well: 20% at 23 nm, approaching each other at the plateau region close to 100 nm [27]. Only one study has reported efficiency of 72% at 100 nm depending on the solution and the dilution [48]. In our study the efficiency was even lower (52%). It is possible that the highly charged atomized salt particles have high losses until their counting, or their crystalized structure results in high contact angles and thus low counting efficiencies [46].

The same figures also plot fittings (Equation (8)) to the experimental data for the following cases:

- *Salt efficiencies:* The counting efficiencies with salt particles.
- *Low efficiencies:* The lowest counting efficiency with the non-salt materials—for the PNC<sub>10</sub>, the manufacturer's PAO data, and for the PNC<sub>23</sub> the soot (or graphite or silver) data.
- *High efficiencies:* The highest counting efficiencies—for the PNC<sub>10</sub> our measured silver (or soot or graphite), and for PNC<sub>23</sub> the manufacturer's PAO data.

These cases were chosen in order to estimate the measurement uncertainty due to differences in calibration procedures. These curves will be used in subsequent sections.

Each material has advantages and disadvantages, as summarized elsewhere [27]. Different criteria can be used for the selection of the appropriate one. For example, electro sprayed PAO particles are spherical with minimum contribution of multiply charged particles. Salt particles are probably the safest to use, but the least relevant to combustion processes, as the particles found in vehicles' exhaust. Soot particles are agglomerates, with properties that depend on the combustion parameters [28,42]. The impact of multiply charged particles can be kept low (<2%) with appropriate selection of the mean size of the generated size distribution [28].

### 3.2. Monodisperse Calibration of VPR

Figure 6 presents the  $PCRF$  ratios to the average  $PCRF$  of 30 nm, 50 nm, 100 nm, over different sizes, which is the inverse of the VPR efficiency (Equation (6)). The setup of Figure 3 was used, and Equation (4) was applied. The tests were conducted with  $PCRF$  100. Higher  $PCRF$ s have higher  $PCRF$  ratios at smaller sizes, because higher dilutions and  $PCRF$ s are achieved with lower rotating speeds which increase the diffusional losses for rotating disc type diluters [49].

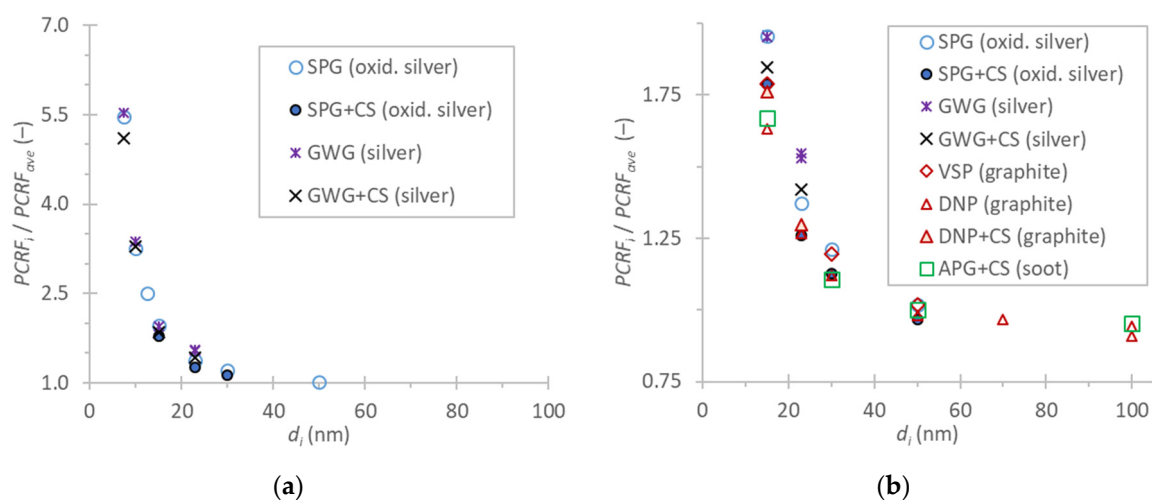


**Figure 6.**  $PCRF$  ratio to  $PCRF_{ave}$  at different sizes (inverse of Equation (6)). The VPR was used with  $PCRF$  100: (a) silver particles; (b) all materials. Lines give fittings to the experimental data of “high” and “low” efficiencies (inverse of  $PCRF$ s).

Figure 6a presents the results with silver particles. Comparing the GWG silver with and without CS, a small difference can be seen. The thermally treated particles have lower  $PCRF$  ratio. The same applies to the SPG oxidized silver particles. However, the differences are very small and within the experimental uncertainty that different setups can have. For example, at 7.5 nm the difference is 0.4 units, but the 10% uncertainty is 0.5 units for a  $PCRF$  ratio of five. The reason for these differences was not further investigated. Even though we do not expect evaporation of the silver particles at the temperature of the VPR at 350 °C, decomposition of the oxidized silver particles, which happens already from 200 °C is possible. Restructuring and sintering cannot be excluded as well, which may result in smaller particles and/or lower number concentrations. Even a 1–2 nm shift would bring the silver particles to the expected curve. The impact of sintering on silver aggregate particles (>50 nm) can start even at low temperatures [50,51], but the impact should be small for particles <20 nm [52]. A recent study with the same SPG generator as in our study and similar settings found that the particles were not completely spherical when air was used as carrier gas [31]. The same study also found that after sintering the actual size of particles, as determined by TEM images, was smaller than the one measured by SMPS (GMD 8 nm vs. 11 nm).

Figure 6b compares more materials in the size range of interest of the regulation (15 nm to 100 nm). Not all materials could cover all sizes. Larger sizes could be generated at adequate concentrations with graphite and soot generators, while smaller particles were generated with silver generators. In general, the agreement was good, in particular, at sizes 50 nm or larger. At 15 nm the scatter was quite high: from 1.63 to 1.85 for the thermally stable particles and 1.95 for silver particles not thermally treated. The maximum difference from the manufacturer’s value was 0.18 for the thermally treated silver and 0.28 for the non-treated silver. The measurement uncertainty was around 0.18 (10%) at this size. For the 23 nm point, there were no data from the manufacturer. The thermally stable particles ranged from 1.27 to 1.42, while the non-treated silver particles ranged from 1.37 to 1.54. At

larger sizes the non-treated silver particles overlapped with the rest materials. This was expected, because the size dependency of the losses is not as steep as with small particles. The data were fitted (Equation (8)) to the following cases:

- *Low efficiencies:* For this scenario, for the VPR, our silver data without thermal pre-treatment were used. Note that high *PCRF* translates to low efficiency (see Equation (6)).
- *High efficiencies:* For this scenario, for the VPR, the manufacturer's soot efficiencies were selected.

The present results confirm that the current requirement in the regulation (i.e., to calibrate with thermally stable particles) is adequate, but has to be checked by the calibration institute.

### 3.3. Monodisperse Calibration of LABS

The efficiency of a particle number system is practically the product of the efficiencies of the PNC and the VPR. Figure 7 compares how the theoretical and measured efficiencies of the complete system are compared with two scenarios, which represent the lowest and highest efficiencies of the complete system:

- *Low efficiencies:* For this scenario, the "low" PNC and "low" VPR curves were multiplied.
- *High efficiencies:* For this scenario, the "high" PNC and "high" VPR curves were multiplied.

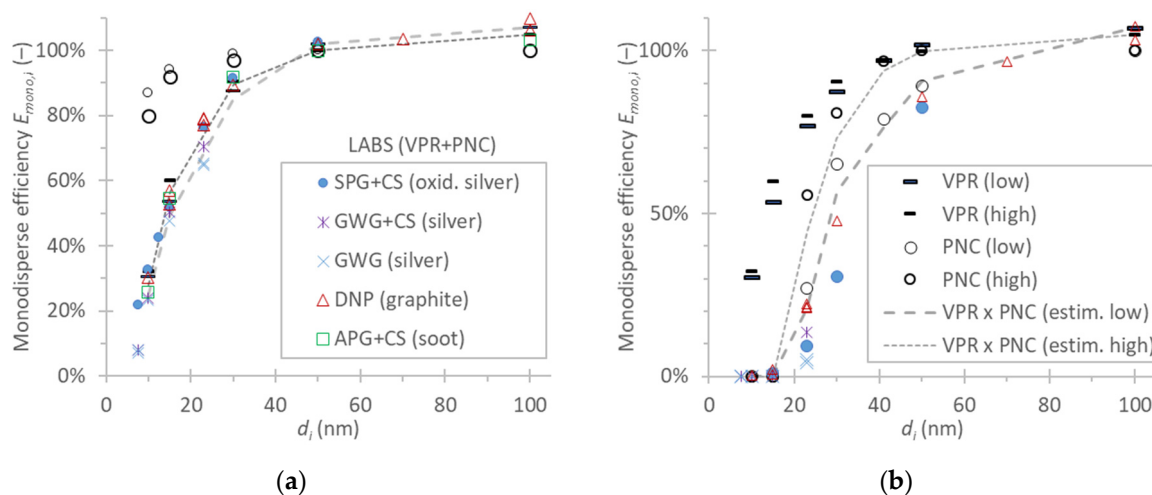


**Figure 7.** Comparison of monodisperse calibration in parts (VPR or PNC) or as a complete system (LABS = VPR + PNC): (a) 10 nm; (b) 23 nm. The *PCRF* of the LABS was 100. Note that the legend is split in the two panels.

Figure 7a presents the two scenarios for the 10 nm system. The *PCRF* of the LABS was 100, and the manufacturer's value was applied in the calculations. The  $PNC_{10}$  and VPR low and high efficiencies as selected above are plotted. The estimated efficiencies of the complete system multiplying the lowest and highest efficiencies of the PNC and VPR (Equation (10)) ( $VPR \times PNC$  curves) are also given. The measured efficiencies of the complete system  $LABS_{10}$ , measured with oxidized silver particles downstream of a catalytic stripper (CS) are also plotted. The  $LABS_{10}$  complete system experimental data with thermally treated silver or oxidized silver or soot or graphite agree well with the estimated efficiencies (mainly with the high scenario) ( $VPR \times PNC$ ). The silver particles not treated are slightly lower, probably due to their higher losses as discussed in Figure 6. The results also highlight that, for 10 nm systems, the efficiency is practically determined by the VPR efficiency curve, while the  $PNC_{10}$  has minor impact. The reason is the low VPR efficiency at 10–15 nm, where the  $PNC_{10}$  already has high efficiency (>80%).

Figure 7b presents data for the 23 nm system, in the same format as Figure 7a. In contrast to 10 nm systems, for 23 nm systems ( $LABS_{23}$ ) the efficiency is determined by

the PNC<sub>23</sub>, and not the VPR. The second point is that the “low” and “high” scenarios have quite large differences, due to the high dependency of the PNC efficiency on the material. The agreement of the graphite particles with the theoretical curve is very good. No data were available with soot particles. However, the experimental results with silver or oxidized silver are lower than the “low” curve. This could be due to the reasons discussed in Figure 6; the losses are higher for these particles, which might have been affected in the VPR. A study showed that the counting efficiencies of a 23 nm PNC changed after sintering the silver particles, while the effect for the 10 nm PNC was negligible [52]. Nevertheless, as the fittings to the data did not fully capture all “low” efficiency cases, this might have contributed to the differences (Figures 5 and 6).

The previous results also show that calibration in parts or as a complete unit are equivalent under the following conditions:

- The material that is used for the complete unit should be the same as with the one used for the separate parts, or at least it should be proven to be equivalent. It is also clear that the material used for the PNC calibration should be thermally pre-treated to simulate the VPR that is upstream of the PNC. For the VPR calibration it is critical to ensure the thermal stability of the calibration particles.
- The concentrations need to be appropriate for the calibration. For example, a PNC measures accurately with low need for coincidence (or dead time) corrections in the  $1 \times 10^2$  to  $5 \times 10^3$  #/cm<sup>3</sup> range. The complete system, with a dilution 100, would need  $1 \times 10^4$  to  $5 \times 10^5$  #/cm<sup>3</sup> range. However, typically the concentration at the outlet of the classifier is  $10^4$  #/cm<sup>3</sup>, resulting in higher uncertainties for the calibration of the complete system as a unit.
- The sizes selected should be common for a direct comparison. Current regulations (e.g., UNECE GTR 15 and Regulation (EU) 2017/1151) have different sizes, requiring fittings of the experimental data to estimate the efficiencies at other sizes.

### 3.4. Polydisperse Checks of LABS

Figure 8 presents comparisons of estimated and experimental data measuring polydisperse aerosol (setup of Figure 4). The PCRF of the LABS was 100, and the manufacturer’s value was applied in the calculations. The experimental data included silver, soot, graphite, and salt particles. The estimated efficiencies of the complete system (LABS or VPR + PNC) to polydisperse aerosol with various size distributions with GMDs 15–110 nm are given for the following scenarios.

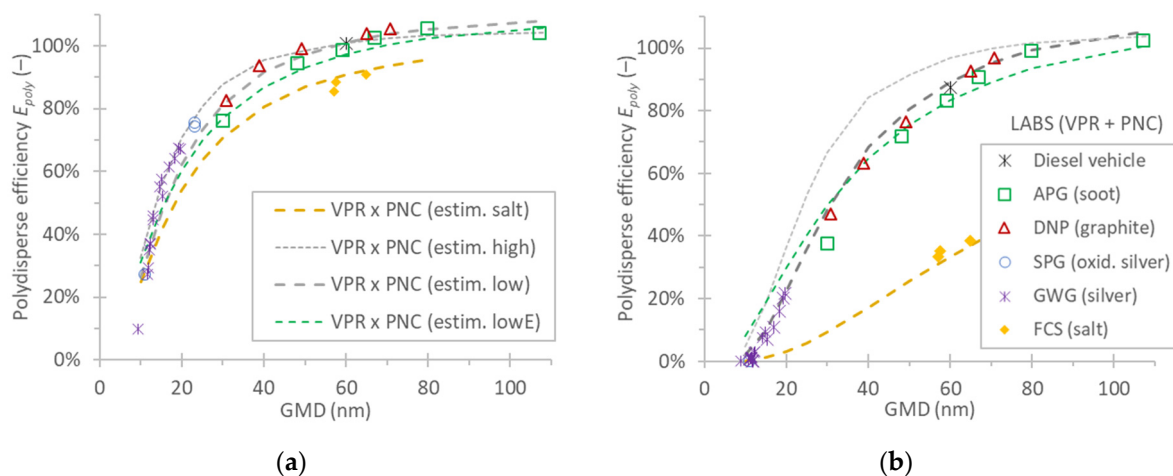


**Figure 8.** Comparison of estimated ( $VPR \times PNC$ ) and measured ( $LABS = VPR + PNC$ ) system efficiency with polydisperse aerosol: (a) 10 nm system; (b) 23 nm system. Assumed geometric standard deviation (GSD) for salt 1.85, GSD for low and high scenarios 1.5–1.6, GSD for LowE scenario 2.1. The PCRF of the LABS was 100. Note that the legend is split in the two panels.

- *High*: The “high” efficiencies of the LABS (both VPR and PNC), assuming size distributions with GSD 1.5–1.6.
- *Low*: The “low” efficiencies of the LABS (both VPR and PNC), assuming size distributions with GSD 1.5–1.6.
- *LowE*: The “low” efficiencies of the LABS (both VPR and PNC), using GSD 1.7–2.1 that matched the experimental GSDs.
- *Salt*: The “low” VPR scenario but using PNC “salt” efficiencies and GSD 1.85 that matched the experimental salt GSD.

Starting with the 10 nm system (Figure 8a), in general, there was a good agreement between experimental and theoretical data. The “low” and “high” scenarios were quite close to each other, as with the monodisperse aerosol (Figure 7a). A small difference at GMD 30 nm for the soot particles was due to the wide GSD of the generated particles (GSD = 2.1) which better matched the “LowE” curve. The silver particles also matched the theoretical curves. The present results also include the uncertainty of the reference instrumentation, which consisted of a PNC<sub>Ref</sub> and a dilution system (Figure 4). The dilution system had losses at small sizes that were taken into account in the results presented (around 25% at 10–15 nm), as discussed in Section 2.2.7.

Figure 8b plots the same information for the 23 nm system. The experimental results were also close to the estimated curves (“low” scenario). The reason is that the low efficiencies were based on soot particles. The two scenarios have relatively big differences, as was also the case with the monodisperse aerosol, due to the overestimation of the counting efficiency of the PNC counting efficiency with PAO particles (Figure 7b). These results highlight that the calibration material should be the same or similar to what is intended to be measured. The present results support the use of soot, graphite or silver particles. For silver particles without thermal pre-treatment there were concerns with the monodisperse tests that the VPR might change their size and result in higher losses. Here, with the polydisperse tests, this effect was not evident, but as mentioned previously, the uncertainty at the 10–15 nm range is high. For salt particles, the lower counting efficiencies of the PNCs (Figure 5) were also depicted in the polydisperse size distributions, which were much lower than the rest materials.

Comparing Figure 8 with Figure 7 it can be concluded that the polydisperse efficiency at a specific GMD is very similar to the monodisperse at the same monodisperse diameter  $d_i$  (around –5% for the 10 nm system, –10% for the 23 nm system). This applies for systems with sigmoid like efficiency curve, as in our case. For systems depending on the power of the diameter (e.g., diffusion chargers) the polydisperse efficiency may be 10–20% higher depending on the exponent and GSD [53,54].

The important message is that the 50% polydisperse efficiency of 10 nm systems (LABS<sub>10</sub>) is achieved when the inlet size distributions have GMD around 15 nm, while of 23 nm systems (LABS<sub>23</sub>) with GMD around 30 nm. The 85% efficiency is achieved at 30 nm and 60 nm, respectively.

### 3.5. Combining Information of PNC<sub>10</sub> and PNC<sub>23</sub>

One topic of interest is whether the combination of the two PNCs (23 nm and 10 nm) sampling from the same VPR, can give useful information. Figure 9a compares the ratio of the two PNCs with the GMD of the size distribution that is being measured. The experimental data with soot (squares), graphite (triangles), and diesel (asterisk) particles are in good agreement with the expected (estimated) trend (curve “low”). However, the uncertainty is quite high, as a system with lower losses (curve “high”) would have significantly different results, in particular below 50 nm. The conclusions that can be extracted from this graph are:

- Ratio <110% (i.e., differences between the two PNCs <10%) typically means GMDs >40 nm.
- Ratio >150% translates to GMD <40 nm.

- GMDs <30 nm have extremely high uncertainty on the ratios because the LABS<sub>23</sub> measures very low emissions.

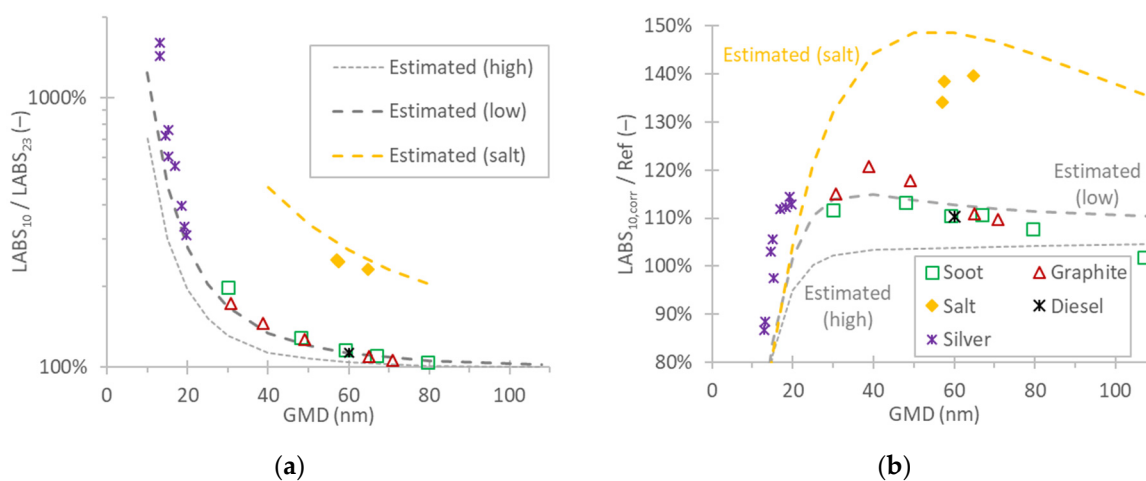


**Figure 9.** Comparison of estimated and measured data for polydisperse aerosol: (a) ratio of 10 nm to 23 nm systems; (b) corrected 10 nm system concentration to reference. Note that the legend is split in the two panels.

It should be emphasized again, that the methodology works only if the efficiencies of the material that is tested are known. For example, the ratio of salt particles is much different than the one for soot (e.g., for GMD 60 nm the ratio is 250% for salt, but 120% for the rest materials).

Figure 9b compares how the correction for sub-23 nm particle losses based on the two PNCs works. This correction (Equations (11) and (12)) is compared with experimental data and the estimated result based on the theoretical responses (polydisperse efficiencies) of the two systems. The results are plotted compared to the reference instrument. For a system with high efficiencies the correction works very well down to 20 nm. Below this size, the 23 nm system measures close to zero and the correction with the 15 nm *PCRF* underestimates the losses. For a system with higher losses (lower efficiencies), the experimental and estimated data agree and show that the correction overestimates the emissions around 10%. The reason is that the 15 nm *PCRF* is high and overcorrects for large GMDs. The correction does not work for salt particles due to the high uncertainty of the efficiencies with salt particles and the very low efficiencies of the  $PNC_{23}$  below 50 nm.

It should be added that the <10% difference at the whole range of GMDs >20 nm is a positive result. Without any correction, the true emissions are underestimated >15% at GMDs of 30 nm and reach 40% at 20 nm (see Figure 8a). Furthermore, with this correction, the differences of systems with high differences in penetration curves, such as the “low” and “high”, remain within 10% of each other.

#### 4. Conclusions

In this study, the effect of the calibration material was studied on the parts of a particle number system: the volatile particle remover (VPR) and two particle number counters (PNC) with cut-off sizes at 23 nm and 10 nm. The results showed that for VPR’s calibration it is crucial to have thermally stable particles, something already prescribed in the regulation. For 10 nm PNCs the impact of the material was small, with salt having lower efficiencies around 5–10%. For 23 nm PNCs the differences were very large: at 23 nm salt had 0% efficiency, while emery oil (PAO) had 56% efficiency. Silver, soot and graphite were in between. The scatter of the efficiencies of the soot particles was high (20–35%). Possible reasons were the thermal pre-treatment, the rich or lean combustion and the size distribution of the generated particles (multiple charge effect). Combining the

efficiencies of the VPR and PNC gave similar results with the efficiencies of the complete system when it was calibrated as a unit. However, it was concluded that (i) the calibration sizes for PNC and VPR need to be the same (in order to avoid fitting of efficiency curves); (ii) the material should be thermally stable also for the PNC calibration and representative of the application that is intended to be used; (iii) the concentration levels should be appropriate for the application. Under these conditions, the comparison of the estimated efficiencies for various size distributions (polydisperse aerosol) was in good agreement with the experimental data. Different materials had different advantages and disadvantages. For example, electrosprayed emery oil had low levels of multiply charged particles, but it was not representative of the intended use of the PNC. Soot on the other hand had high scatter of the results, but on average matched well with the intended use (vehicle exhaust). Silver generators produced adequate concentrations for small sizes and graphite generators for larger sizes. Graphite particles did not need any thermal pre-treatment, while the results showed that silver particles might need thermal pre-treatment. Salt particles were the least representative leading to high deviations from the rest materials.

The results revealed that the 10 nm and 23 nm systems have 50% efficiency for size distributions with geometric mean diameters (GMDs) around 15 nm and 30 nm, respectively. The efficiency of the complete system was determined by the VPR for the 10 nm systems and by the PNC for the 23 nm systems. The ratio of the 10 nm and 23 nm PNCs gave a rough estimation of the GMD of the measured size distribution. Due to the high uncertainties, this index should be indicative only for GMDs larger or smaller than 40 nm. Finally, it was demonstrated that correcting the results for sub-23 nm particle losses when using the two PNCs measuring from the same VPR is possible with an error of up to 10% from GMDs >20 nm.

**Author Contributions:** Conceptualization, B.G.; formal analysis, B.G., A.M.; writing—original draft preparation, B.G.; writing—review and editing, A.M. All authors have read and agreed to the published version of the manuscript.

**Funding:** This research received no external funding.

**Institutional Review Board Statement:** Not applicable.

**Informed Consent Statement:** Not applicable.

**Data Availability Statement:** Data available from the corresponding author upon request.

**Acknowledgments:** The authors would like to acknowledge AVL (Christos Dardiotis, Roman Davok) for providing the APG, Catalytic Instruments (Martin Irwin, Hans-Joachim Schulz) for providing the silver generator, and Topas (Stefano Somaschi, Stephan Grosse) for providing the salt generator. Special acknowledgments to Lesueur for the construction and operation of the glowing wire generator.

**Conflicts of Interest:** The authors declare no conflict of interest.

**Disclaimer:** The opinions expressed in this manuscript are those of the authors and should not in no way be considered to represent an official opinion of the European Commission. Mention of trade names or commercial products does not constitute endorsement or recommendation by the authors or the European Commission.

## References

1. Giechaskiel, B.; Maricq, M.; Ntziachristos, L.; Dardiotis, C.; Wang, X.; Axmann, H.; Bergmann, A.; Schindler, W. Review of Motor Vehicle Particulate Emissions Sampling and Measurement: From Smoke and Filter Mass to Particle Number. *J. Aerosol Sci.* **2014**, *67*, 48–86. [[CrossRef](#)]
2. Giechaskiel, B.; Melas, A.; Martini, G.; Dilara, P. Overview of Vehicle Exhaust Particle Number Regulations. *Processes* **2021**, *9*, 2216. [[CrossRef](#)]
3. Lobo, P.; Durdina, L.; Brem, B.T.; Crayford, A.P.; Johnson, M.P.; Smallwood, G.J.; Siegerist, F.; Williams, P.I.; Black, E.A.; Llamedo, A.; et al. Comparison of Standardized Sampling and Measurement Reference Systems for Aircraft Engine Non-Volatile Particulate Matter Emissions. *J. Aerosol Sci.* **2020**, *145*, 105557. [[CrossRef](#)]

4. Lahde, T.; Giechaskiel, B.; Martini, G. Development of Measurement Methodology for Sub 23 nm Particle Number (PN) Measurements. *SAE Int. J. Adv. Curr. Prac. Mobil.* **2020**, *3*, 551–560. [[CrossRef](#)]
5. Samaras, Z.; Rieker, M.; Papaioannou, E.; van Dorp, W.F.; Kousoulidou, M.; Ntziachristos, L.; Andersson, J.; Bergmann, A.; Hausberger, S.; Keskinen, J.; et al. Perspectives for Regulating 10 nm Particle Number Emissions Based on Novel Measurement Methodologies. *J. Aerosol Sci.* **2022**, *162*, 105957. [[CrossRef](#)]
6. Woodburn, J.; Bielaczyc, P.; Giechaskiel, B. *A Technical Overview of Particulate Exhaust Emissions in the Post-RDE Era*; Technical Paper 2022-01-1021; SAE International: Warrendale, PA, USA, 2022. [[CrossRef](#)]
7. Boger, T.; Rose, D.; He, S.; Joshi, A. Developments for Future EU7 Regulations and the Path to Zero Impact Emissions—A Catalyst Substrate and Filter Supplier’s Perspective. *Transp. Eng.* **2022**, *10*, 100129. [[CrossRef](#)]
8. Samaras, Z.C.; Kontses, A.; Dimaratos, A.; Kontses, D.; Balazs, A.; Hausberger, S.; Ntziachristos, L.; Andersson, J.; Ligterink, N.; Aakko-Saksa, P.; et al. *A European Regulatory Perspective towards a Euro 7 Proposal*; Technical Paper 2022-37-0032; SAE International: Warrendale, PA, USA, 2022. [[CrossRef](#)]
9. Giechaskiel, B.; Bonnel, P.; Perujo, A.; Dilara, P. Solid Particle Number (SPN) Portable Emissions Measurement Systems (PEMS) in the European Legislation: A Review. *Int. J. Environ. Res. Public Health* **2019**, *16*, 4819. [[CrossRef](#)] [[PubMed](#)]
10. Giechaskiel, B.; Lähde, T.; Melas, A.D.; Valverde, V.; Clairotte, M. Uncertainty of Laboratory and Portable Solid Particle Number Systems for Regulatory Measurements of Vehicle Emissions. *Environ. Res.* **2021**, *197*, 111068. [[CrossRef](#)] [[PubMed](#)]
11. Giechaskiel, B.; Lähde, T.; Suarez-Bertoa, R.; Valverde, V.; Clairotte, M. Comparisons of Laboratory and On-Road Type-Approval Cycles with Idling Emissions. Implications for Periodical Technical Inspection (PTI) Sensors. *Sensors* **2020**, *20*, 5790. [[CrossRef](#)]
12. Melas, A.; Selleri, T.; Suarez-Bertoa, R.; Giechaskiel, B. Evaluation of Solid Particle Number Sensors for Periodic Technical Inspection of Passenger Cars. *Sensors* **2021**, *21*, 8325. [[CrossRef](#)] [[PubMed](#)]
13. Melas, A.; Selleri, T.; Suarez-Bertoa, R.; Giechaskiel, B. Evaluation of Measurement Procedures for Solid Particle Number (SPN) Measurements during the Periodic Technical Inspection (PTI) of Vehicles. *Int. J. Environ. Res. Public Health* **2022**, *19*, 7602. [[CrossRef](#)]
14. Boveroux, F.; Cassiers, S.; Buekenhoudt, P.; Chavatte, L.; De Meyer, P.; Jeanmart, H.; Verhelst, S.; Contino, F. *Feasibility Study of a New Test Procedure to Identify High Emitters of Particulate Matter during Periodic Technical Inspection*; Technical Paper 2019-01-1190; SAE International: Warrendale, PA, USA, 2019. [[CrossRef](#)]
15. Marshall, I. *Particle Number Counter Calibration Procedures*; Report ED47382004/PNC; AEA (Ricardo): Didcot, UK, 2007; Available online: <https://unece.org/DAM/trans/doc/2008/wp29grpe/PMP-PNC-CalibrationProcedure.pdf> (accessed on 24 October 2022).
16. Sandbach, E. *Volatile Particle Remover Calibration and Validation Procedures*; Report ED47382004/VPR; AEA (Ricardo): Didcot, UK, 2007; Available online: <https://unece.org/DAM/trans/doc/2008/wp29grpe/PMP-VPR-CalibrationProcedure.pdf> (accessed on 24 October 2022).
17. Bielaczyc, P.; Merkisz, J.; Pajdowski, P.; Woodburn, J. Correlation between Two Commercially Available PMP-Compliant Particle Number Counting Systems. *Combust. Engines* **2012**, *149*, 10–21. [[CrossRef](#)]
18. Kim, H.; Lee, J. Quantitative Analysis of Vehicle Particle Emission by Using Calibrated CPC System. *J. Mech. Sci. Technol.* **2011**, *25*, 2959–2967. [[CrossRef](#)]
19. Giechaskiel, B.; Mamakos, A.; Andersson, J.; Dilara, P.; Martini, G.; Schindler, W.; Bergmann, A. Measurement of Automotive Nonvolatile Particle Number Emissions within the European Legislative Framework: A Review. *Aerosol Sci. Technol.* **2012**, *46*, 719–749. [[CrossRef](#)]
20. Khan, M.Y.; Sharma, S.; Liew, C.M.; Joshi, A.; Barnes, D.; Scott, N.; Mensen, B.; Cao, T.; Li, Y.; Shimpi, S.A.; et al. Comparison of Full Flow Dilution, Partial Flow Dilution, and Raw Exhaust Particle Number Measurements. *Emiss. Control Sci. Technol.* **2018**, *4*, 103–112. [[CrossRef](#)]
21. Giechaskiel, B.; Woodburn, J.; Szczotka, A.; Bielaczyc, P. *Particulate Matter (PM) Emissions of Euro 5 and Euro 6 Vehicles Using Systems with Evaporation Tube or Catalytic Stripper and 23 nm or 10 nm Counters*; Technical Paper 2020-01-2203; SAE International: Warrendale, PA, USA, 2020. [[CrossRef](#)]
22. Giechaskiel, B.; Lähde, T.; Schwelberger, M.; Kleinbach, T.; Roske, H.; Teti, E.; van den Bos, T.; Neils, P.; Delacroix, C.; Jakobsson, T.; et al. Particle Number Measurements Directly from the Tailpipe for Type Approval of Heavy-Duty Engines. *Appl. Sci.* **2019**, *9*, 4418. [[CrossRef](#)]
23. Giechaskiel, B.; Lähde, T.; Gandi, S.; Keller, S.; Kreutziger, P.; Mamakos, A. Assessment of 10-nm Particle Number (PN) Portable Emissions Measurement Systems (PEMS) for Future Regulations. *IJERPH* **2020**, *17*, 3878. [[CrossRef](#)]
24. Giechaskiel, B.; Schwelberger, M.; Kronlund, L.; Delacroix, C.; Locke, L.A.; Khan, M.Y.; Jakobsson, T.; Otsuki, Y.; Gandi, S.; Keller, S.; et al. Towards Tailpipe Sub-23 Nm Solid Particle Number Measurements for Heavy-Duty Vehicles Regulations. *Transp. Eng.* **2022**, *9*, 100137. [[CrossRef](#)]
25. Terres, A.; Giechaskiel, B.; Nowak, A.; Ebert, V. Calibration Uncertainty of 23 nm Engine Exhaust Condensation Particle Counters with Soot Generators: A European Automotive Laboratory Comparison. *Emiss. Control Sci. Technol.* **2021**, *7*, 124–136. [[CrossRef](#)]
26. Kiwull, B.; Wolf, J.-C.; Niessner, R. Response Characteristics of PMP Compliant Condensation Particle Counters toward Various Calibration Aerosols. *Aerosol Sci. Technol.* **2015**, *49*, 98–108. [[CrossRef](#)]

27. Wang, X.; Caldwell, R.; Sem, G.J.; Hama, N.; Sakurai, H. Evaluation of a Condensation Particle Counter for Vehicle Emission Measurement: Experimental Procedure and Effects of Calibration Aerosol Material. *J. Aerosol Sci.* **2010**, *41*, 306–318. [[CrossRef](#)]
28. Giechaskiel, B.; Wang, X.; Horn, H.-G.; Spielvogel, J.; Gerhart, C.; Southgate, J.; Jing, L.; Kasper, M.; Drossinos, Y.; Krasenbrink, A. Calibration of Condensation Particle Counters for Legislated Vehicle Number Emission Measurements. *Aerosol Sci. Technol.* **2009**, *43*, 1164–1173. [[CrossRef](#)]
29. Khan, M.Y.; Patel, M.; Scott, N.; Liew, C.M.; Peng, C.; Luo, W.; Rahman, M.; Gramlich, N.; Eames, J.; Phillips, J.A. *Assessment of In-Use Solid Particle Number Measurement Systems against Laboratory Systems*; Technical Paper 2020-01-5074; SAE International: Warrendale, PA, USA, 2020. [[CrossRef](#)]
30. Giechaskiel, B.; Mamakos, A.; Woodburn, J.; Szczotka, A.; Bielaczyc, P. Evaluation of a 10 nm Particle Number Portable Emissions Measurement System (PEMS). *Sensors* **2019**, *19*, 5531. [[CrossRef](#)] [[PubMed](#)]
31. Hammer, T.; Irwin, M.; Swanson, J.; Berger, V.; Sonkamble, U.; Boies, A.; Schulz, H.; Vasilatou, K. Characterising the Silver Particle Generator; a Pathway towards Standardising Silver Aerosol Generation. *J. Aerosol Sci.* **2022**, *163*, 105978. [[CrossRef](#)]
32. TSI Inc. *Model 3752 Condensation Particle Counter Operation Manual, P/N 6011194, Revision D 2022*; TSI: Shoreview, MN, USA, 2022.
33. Giechaskiel, B.; Bergmann, A. On-Site Checks of the Particle Number Measurement Systems with Polydisperse Aerosol. *SAE Int. J. Engines* **2012**, *5*, 649–662. [[CrossRef](#)]
34. Giechaskiel, B.; Lähde, T.; Drossinos, Y. Regulating Particle Number Measurements from the Tailpipe of Light-Duty Vehicles: The next Step? *Environ. Res.* **2019**, *172*, 1–9. [[CrossRef](#)]
35. Helsper, C.; Mölter, W.; Löffler, F.; Wadenpohl, C.; Kaufmann, S.; Wenninger, G. Investigations of a New Aerosol Generator for the Production of Carbon Aggregate Particles. *Atmos. Environment. Part A Gen. Top.* **1993**, *27*, 1271–1275. [[CrossRef](#)]
36. Giechaskiel, B.; Davok, R.; Melz Giovanella, K.; Joergl, H.; Diwald, R.; Schindler, W. Particle Generator (APG): A Soot Generator for the on-Site Checks of Particle Number (PN) Measurement Systems. In Proceedings of the JSAE Annual Congress, SAE, Pacifico, Yokohama, Japan, 24 May 2013.
37. Yli-Ojanperä, J.; Sakurai, H.; Iida, K.; Mäkelä, J.M.; Ehara, K.; Keskinen, J. Comparison of Three Particle Number Concentration Calibration Standards through Calibration of a Single CPC in a Wide Particle Size Range. *Aerosol Sci. Technol.* **2012**, *46*, 1163–1173. [[CrossRef](#)]
38. Maricq, M.M. Examining the Relationship between Black Carbon and Soot in Flames and Engine Exhaust. *Aerosol Sci. Technol.* **2014**, *48*, 620–629. [[CrossRef](#)]
39. Moore, R.H.; Ziemba, L.D.; Dutcher, D.; Beyersdorf, A.J.; Chan, K.; Crumeyrolle, S.; Raymond, T.M.; Thornhill, K.L.; Winstead, E.L.; Anderson, B.E. Mapping the Operation of the Miniature Combustion Aerosol Standard (Mini-CAST) Soot Generator. *Aerosol Sci. Technol.* **2014**, *48*, 467–479. [[CrossRef](#)]
40. Kim, J.; Bauer, H.; Dobovičnik, T.; Hitzenberger, R.; Lottin, D.; Ferry, D.; Petzold, A. Assessing Optical Properties and Refractive Index of Combustion Aerosol Particles Through Combined Experimental and Modeling Studies. *Aerosol Sci. Technol.* **2015**, *49*, 340–350. [[CrossRef](#)]
41. Ess, M.N.; Vasilatou, K. Characterization of a New MiniCAST with Diffusion Flame and Premixed Flame Options: Generation of Particles with High EC Content in the Size Range 30 Nm to 200 Nm. *Aerosol Sci. Technol.* **2019**, *53*, 29–44. [[CrossRef](#)]
42. Mamakos, A.; Khalek, I.; Giannelli, R.; Spears, M. Characterization of Combustion Aerosol Produced by a Mini-CAST and Treated in a Catalytic Stripper. *Aerosol Sci. Technol.* **2013**, *47*, 927–936. [[CrossRef](#)]
43. Durdina, L.; Lobo, P.; Trueblood, M.B.; Black, E.A.; Achterberg, S.; Hagen, D.E.; Brem, B.T.; Wang, J. Response of Real-Time Black Carbon Mass Instruments to Mini-CAST Soot. *Aerosol Sci. Technol.* **2016**, *50*, 906–918. [[CrossRef](#)]
44. Giechaskiel, B.; Melas, A.D. Comparison of Particle Sizers and Counters with Soot-Like, Salt and Silver Particles. *Atmosphere* **2022**, *13*, 1675. [[CrossRef](#)]
45. Giechaskiel, B.; Bergmann, A. Validation of 14 Used, Re-Calibrated and New TSI 3790 Condensation Particle Counters According to the UN-ECE Regulation 83. *J. Aerosol Sci.* **2011**, *42*, 195–203. [[CrossRef](#)]
46. Giechaskiel, B.; Wang, X.; Gilliland, D.; Drossinos, Y. The Effect of Particle Chemical Composition on the Activation Probability in N-Butanol Condensation Particle Counters. *J. Aerosol Sci.* **2011**, *42*, 20–37. [[CrossRef](#)]
47. Mamakos, A.; Giechaskiel, B.; Drossinos, Y. Experimental and Theoretical Investigations of the Effect of the Calibration Aerosol Material on the Counting Efficiencies of TSI 3790 Condensation Particle Counters. *Aerosol Sci. Technol.* **2013**, *47*, 11–21. [[CrossRef](#)]
48. Krasa, H.; Kupper, M.; Schriefl, M.A.; Bergmann, A. Influence of Concentration and Dilution of Atomized Salt Particles on the Counting Efficiency of 23-nm Automotive Condensation Particle Counters. In Proceedings of the 11th International Aerosol Conference, Athens, Greece, 4–9 September 2022.
49. Giechaskiel, B.; Cresnoverh, M.; Jörgl, H.; Bergmann, A. Calibration and Accuracy of a Particle Number Measurement System. *Meas. Sci. Technol.* **2010**, *21*, 045102. [[CrossRef](#)]
50. Harra, J.; Mäkitalo, J.; Siikanen, R.; Virkki, M.; Genty, G.; Kobayashi, T.; Kauranen, M.; Mäkelä, J.M. Size-Controlled Aerosol Synthesis of Silver Nanoparticles for Plasmonic Materials. *J. Nanopart. Res.* **2012**, *14*, 870. [[CrossRef](#)]
51. Ku, B.K.; Maynard, A.D. Generation and Investigation of Airborne Silver Nanoparticles with Specific Size and Morphology by Homogeneous Nucleation, Coagulation and Sintering. *J. Aerosol Sci.* **2006**, *37*, 452–470. [[CrossRef](#)]
52. Tuch, T.; Weinhold, K.; Merkel, M.; Nowak, A.; Klein, T.; Quincey, P.; Stolzenburg, M.; Wiedensohler, A. Dependence of CPC Cut-off Diameter on Particle Morphology and Other Factors. *Aerosol Sci. Technol.* **2016**, *50*, 331–338. [[CrossRef](#)]

- 
53. Fierz, M.; Houle, C.; Steigmeier, P.; Burtscher, H. Design, Calibration, and Field Performance of a Miniature Diffusion Size Classifier. *Aerosol Sci. Technol.* **2011**, *45*, 1–10. [[CrossRef](#)]
  54. Maricq, M.M. Monitoring Motor Vehicle PM Emissions: An Evaluation of Three Portable Low-Cost Aerosol Instruments. *Aerosol Sci. Technol.* **2013**, *47*, 564–573. [[CrossRef](#)]